Revisiting the hysteresis effect in surface energy budgets

Article

Published Version

It is advisable to refer to the publisher's version if you intend to cite from the work. See Guidance on citing.

To link to this article DOI: http://dx.doi.org/10.1002/grl.50385

www.reading.ac.uk/centaur

CentAUR

Central Archive at the University of Reading

Revisiting the hysteresis effect in surface energy budgets

Ting Sun,[1] Zhi-Hua Wang,[2] and Guang-Heng Ni[1]

[1] The hysteresis effect in diurnal cycles of net radiation R_n and ground heat flux G_0 has been observed in many studies, while the governing mechanism remains vague. In this study, we link the phenomenology of hysteresis loops to the wave phase difference between the diurnal evolutions of various terms in the surface energy balance. R_n and G_0 are parameterized with the incoming solar radiation and the surface temperature as two control parameters of the surface energy partitioning. The theoretical analysis shows that the vertical water flux W and the scaled ratio A_s^*/A_T^* (net shortwave radiation to outgoing longwave radiation) play crucial roles in shaping hysteresis loops of R_n and G_0. Comparisons to field measurements indicate that hysteresis loops for different land covers can be well captured by the theoretical model, which is also consistent with Camuffo-Bernadi formula. This study provides insight into the surface partitioning and temporal evolution of the energy budget at the land surface. **Citation:** Sun, T., Z.-H. Wang, and G.-H. Ni (2013), Revisiting the hysteresis effect in surface energy budgets, *Geophys. Res. Lett.*, *40*, 1741–1747, doi:10.1002/grl.50385.

1. Introduction

[2] An integrated earth system model must be able to physically resolve the transfer of energy, water, and tracers across the land-atmosphere interface [*Liang et al.*, 1994; *Sellers et al.*, 1997; *Katul et al.*, 2012]. Partitioning of solar energy at the land surface provides the lower boundary conditions for the atmospheric dynamics of energy and water cycles, and dictates the land-atmospheric interactions [*Mccumber and Pielke*, 1981; *Chen and Dudhia*, 2001]. The surface energy balance (SEB) equation is given by:

$$R_n - G_0 = H + LE, \qquad (1)$$

where R_n, G_0, H, and LE are the net radiation, ground, sensible, and latent heat fluxes, respectively. The left-hand side of equation (1) denotes the available energy received at the land surface, while the right-hand side is the atmospheric energy dispersion through turbulent transport.

[3] While the net radiation and turbulent (sensible and latent) fluxes can be readily measured in the atmospheric boundary layer using standard radiometry and eddy-

covariance technology, respectively, accurate determination of the ground heat flux is more challenging. Historically, G_0 is parameterized as a constant fraction of R_n during a diurnal cycle [*Humes et al.*, 1994]. However, the assumed linear proportionality between R_n and G_0 is not satisfied due to the existence of the hysteresis loop between the two energy fluxes, as observed by numerous researchers in field measurements [*Taesler*, 1980; *Camuffo and Bernardi*, 1982; *Doll et al.*, 1985; *Kustas and Daughtry*, 1990; *Yoshida et al.*, 1990; *Grimmond et al.*, 1991; *Asaeda and Ca*, 1993; *Asaeda et al.*, 1996; *Taha*, 1997; *Anandakumar*, 1999; *Meyn and Oke*, 2009]. The hysteresis effect is essentially due to the existence of phase difference between the diurnal variations of R_n and G_0, which is $\pi/4$ for dry soils. The Camuffo-Bernadi formula was first proposed to characterize the diurnal evolution of G_0 as a function of R_n [*Camuffo and Bernardi*, 1982]:

$$G_0(t) = a_1 R_n(t) + a_2 \frac{\partial R_n(t)}{\partial t} + a_3, \qquad (2)$$

where a_1, a_2, and a_3 are site-specific empirical coefficients. Note that the time derivative of net radiation in equation (2) introduces the phase difference between G_0 and R_n, albeit empirically. *Santanello and Friedl* [2003] discussed the phase lag between G_0 and T_s and found the value varies with soil moisture conditions and equals $\pi/4$ for dry soils. By solving the one-dimensional advection-diffusion equation of coupled heat and liquid water transport, *Gao et al.* [2003, 2010] concluded that the vertical water flux plays a crucial role in regulating the phase lag between G_0 and T_s. Relating the evolution of R_n to that of T_s without phase lag partially explains the hysteresis effect, with G_0 always leading in phase as compared to R_n, which contradicts field observations under certain conditions [e.g., *Camuffo and Bernardi*, 1982; *Anandakumar*, 1999].

[4] In this letter, we revisit the physical mechanisms governing the hysteresis effect between the net radiation and the ground heat flux by focusing on their diurnal wave phase evolution. We propose theoretical parameterization schemes for R_n and G_0 and test them using field experiment data from various land use land cover (LULC) types. A linkage between the proposed scheme and the empirically based Camuffo-Bernadi formula is also established.

2. Theoretical Analysis

2.1. Parameterization of R_n

[5] The net radiation R_n is the sum of incoming and outgoing shortwave and longwave components and can be written as:

$$R_n = (1 - \alpha)S_d + \varepsilon_a \sigma T_a^4 - \varepsilon_s \sigma T_s^4, \qquad (3)$$

where α is the albedo of the ground surface, S_d the incoming shortwave radiation, ε_a the effective emissivity of the

[1]State Key Laboratory of Hydro-Science and Engineering, Department of Hydraulic Engineering, Tsinghua University, Beijing 100084, China.
[2]School of Sustainable Engineering and the Built Environment, Arizona State University, Tempe, AZ 85287, USA.

Corresponding author: Z.-H. Wang, School of Sustainable Engineering and the Built Environment, Arizona State University, Tempe, AZ 85287, USA. (zhwang@asu.edu)
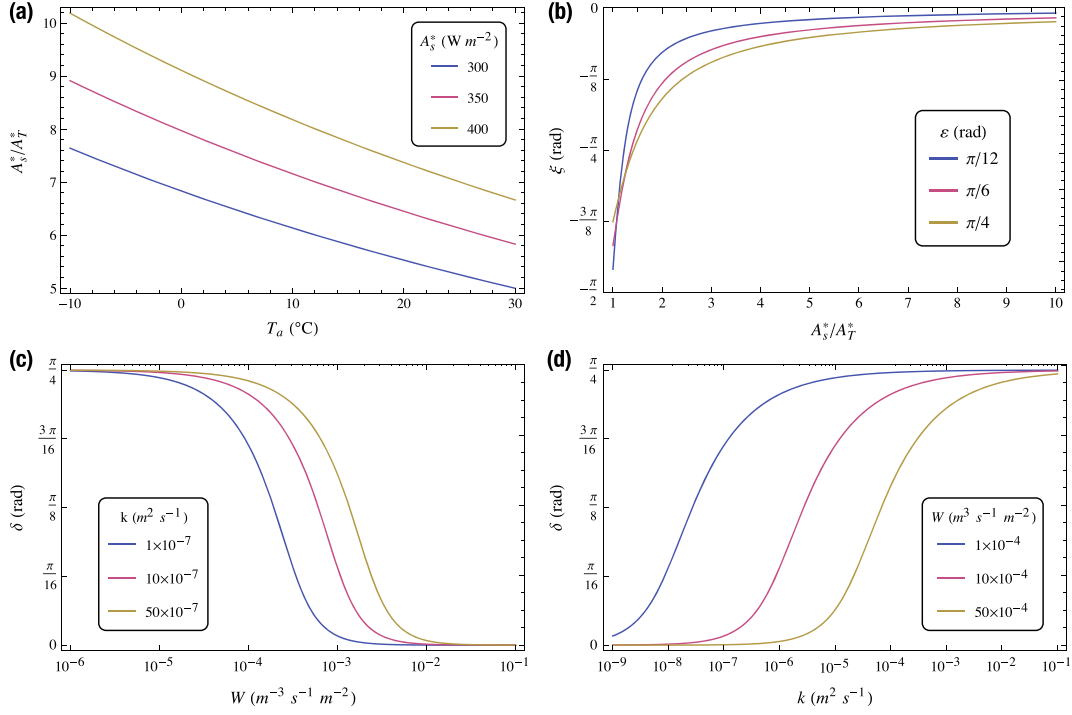
Figure 1. Variation of (a) scale ratio of radiative forcing A_s^*/A_T^* as a function of air temperature T_a, (b) phase lag ξ as a function of scale ratio of A_s^*/A_T^*, (c) phase lag δ as a function of water flux density W with different thermal diffusivity k, and (d) phase lag δ as a function of thermal diffusivity k with different water flux density W.

atmosphere, ε_s the emissivity of the land surface, $\sigma = 5.67$ 10^{-8} (W m^{-2} K^{-4}) the Stefan-Boltzmann constant, T_a the air temperature, and T_s the surface temperature. The incoming longwave radiation is parameterized using the atmospheric temperature [*Brutsaert*, 1975].

[6] During a clear day, the ground first responds to the incoming solar energy with increasing surface temperature T_s, while the response of overlying atmosphere is indirect due to surface heating. Taking S_d and T_s as the control

parameters of SEB and using Taylor expansion, equation (3) can be linearized in terms of S_d and T_s [*Bateni and Entekhabi*, 2012], as

$$R_n = (1-\alpha)S_d + (\varepsilon_a + 3\varepsilon_s)\sigma T_a^4 - 4\varepsilon_s\sigma T_a^3 T_s. \qquad (4)$$

By setting $t = 0$ at sunrise, we first parameterize S_d and T_s using sinusoidal functions occurring at a principle diurnal frequency of the Earth's rotation $\omega = 2\pi/24$ (in rad/h) as:
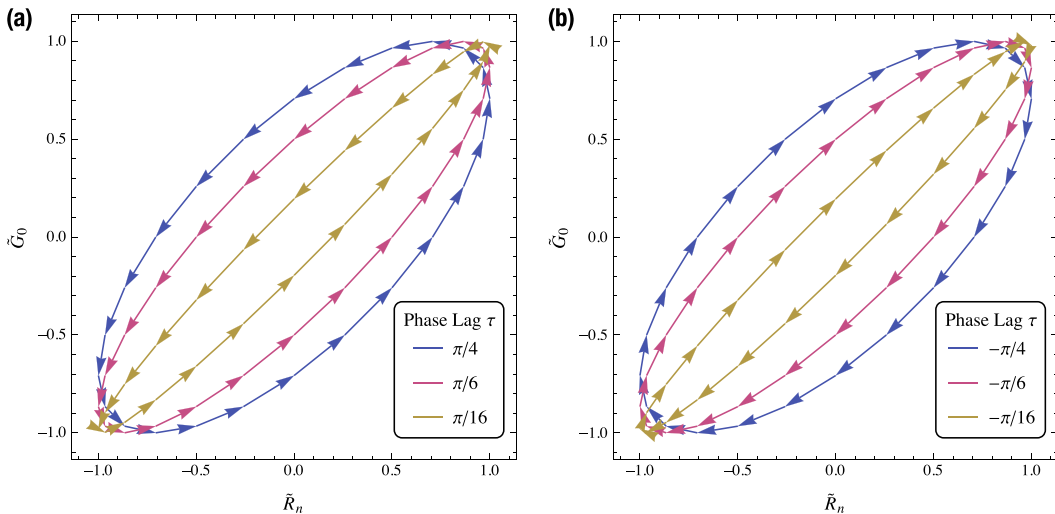

Figure 2. Hysteresis loops between the normalized net radiation $\widetilde{R}_n$ and the normalized ground heat flux $\widetilde{G}_0$, evolving in (a) counterclockwise ($\tau > 0$), and (b) clockwise ($\tau < 0$) directions, respectively. The width of hysteresis loops is regulated by the wave phase difference τ between $\widetilde{R}_n$ and $\widetilde{G}_0$.

$$S_d(t) = A_s \sin(\omega t) + \overline{S}_d, \quad (5)$$

$$T_s(t) = A_T \sin(\omega t - \varepsilon) + \overline{T}_s, \quad (6)$$

where A_s and A_T are amplitudes of daily S_d and T_s variation, respectively, $\overline{S}_d$ the daily mean solar radiation, $\overline{T}_s$ the daily mean temperature, and $\varepsilon \geq 0$ the phase lag between T_s and S_d indicating the response time of ground surface to solar heating. With a simple harmonic at the principle diurnal frequency, it is analogous to the force-restore method [*Bhumralkar*, 1975]. In practice, sinusoidal variation mimics actual evolutions of T_s and S_d for clear days with reasonable accuracy [*Gao et al.*, 2003]. For better representation of diurnal cycles of T_s and S_d, Fourier series including more harmonic functions with higher frequencies can be used [*Gentine et al.*, 2010; 2011; 2012] in equations (5) and (6), without qualitatively altering our subsequent analysis. Substituting equations (5) and (6) into equation (4), we have

$$R_n(t) = A_R \sin(\omega t - \xi) + R'_n, \quad (7)$$

where A_R is the amplitude of net radiation, ξ the phase lag between R_n and S_d, and R'_n the residual term. The three terms in equation (7) are given by

$$A_R = [(1-\alpha)^2 A_S^2 - 8(1-\alpha)\varepsilon_s \sigma T_a^3 A_S A_T \cos(\varepsilon) \quad (8)$$
$$+ 16\varepsilon_s^2 \sigma^2 T_a^6 A_T^2]^{-1/2},$$

$$\xi = \arctan\left[\frac{4\varepsilon_s \sigma T_a^3 A_T \sin(\varepsilon)}{4\varepsilon_s \sigma T_a^3 A_T \cos(\varepsilon) - (1-\alpha)A_S}\right], \quad (9)$$

and

$$R'_n = (1-\alpha)\overline{S}_d + (\varepsilon_a + 3\varepsilon_s)\sigma T_a^4 - 4\varepsilon_s \sigma T_a^3 \overline{T}_s, \quad (10)$$

respectively. Excluding R'_n from equation (7) and successively normalizing R_n by the amplitude A_R, we have the normalized net radiation $\widetilde{R}_n$ as:

$$\widetilde{R}_n(t) = \sin(\omega t - \xi). \quad (11)$$

2.2. Parameterization of G_0

[7] Following *Gao et al.* [2003, 2010], we consider the one-dimensional advection-diffusion equation in the soil:

$$\frac{\partial T}{\partial t} = k\frac{\partial^2 T}{\partial z^2} + W\frac{\partial T}{\partial z}, \quad (12)$$

where T is the soil temperature at a reference depth z (positive downward), k is the soil thermal diffusivity, and $W = \partial k/\partial z - (C_W/C_g)w\varphi$ is the soil water flux density [*Ren et al.*, 2000] with C_W the volumetric heat capacity of water, C_g the volumetric heat capacity of soil, w the pore water velocity, and φ the volumetric soil water content. Taking the surface temperature given by equation (6) as the upper boundary condition, solutions of soil temperature and heat flux of equation (12) are

Table 1. Description of the Experiment Sites

Surface Type	Surface Wetness	Period	Site Name	Location (Coordinate)	G_0 Calculation	Additional Information[a]
Green Roof	Wet	July 2012	Tsinghua Green Roof [*Sun et al.*, 2013]	Beijing, China (40.00 N, 116.33 E)	Heat Storage	$C_g = 1.0 \times 10^6$ $z = 0.02$
Natural Soil	Moderate	May 2012	Korla Cotton Field	Xinjiang, China (41.58 N, 86.16 E)	Energy Residual	$h = 5.0$
Black Roof	Dry	12–13 Sept. 2012	PPPL Black Roof	New Jersey, U.S. (40.35 E, 74.64 W)	Heat Storage	$C_g = 2.0 \times 10^6$ $z = 0.01$
White Roof	Dry	12–13 Sept. 2012	PPPL White Roof	New Jersey, U.S. (40.35 N, 74.60 W)	Heat Storage	$C_g = 2.0 \times 10^6$ $z = 0.01$
Grass Land	Wet	Oct. 2010	Broadmead Grass Land [*Wang and Bou-Zeid*, 2012]	New Jersey, U.S. (40.35 N, 74.60 W)	Heat Storage	$C_g = 1.3 \times 10^6$ $z = 0.08$
Suburban Area	Moderate	Oct. 2010	EQuad Ballast Roof [*Wang et al.*, 2011]	New Jersey, U.S. (40.35 N, 74.65 W)	Energy Residual	$h = 23.2$

[a]The dry soil volumetric heat capacity C_g (in J m^{-3} K^{-1}) and the depth z (in m) at which soil heat fluxes G_z were measured are provided for sites using heat storage method. For sites where the energy residual method is used, the height of eddy-covariance instruments h (in m) is reported.
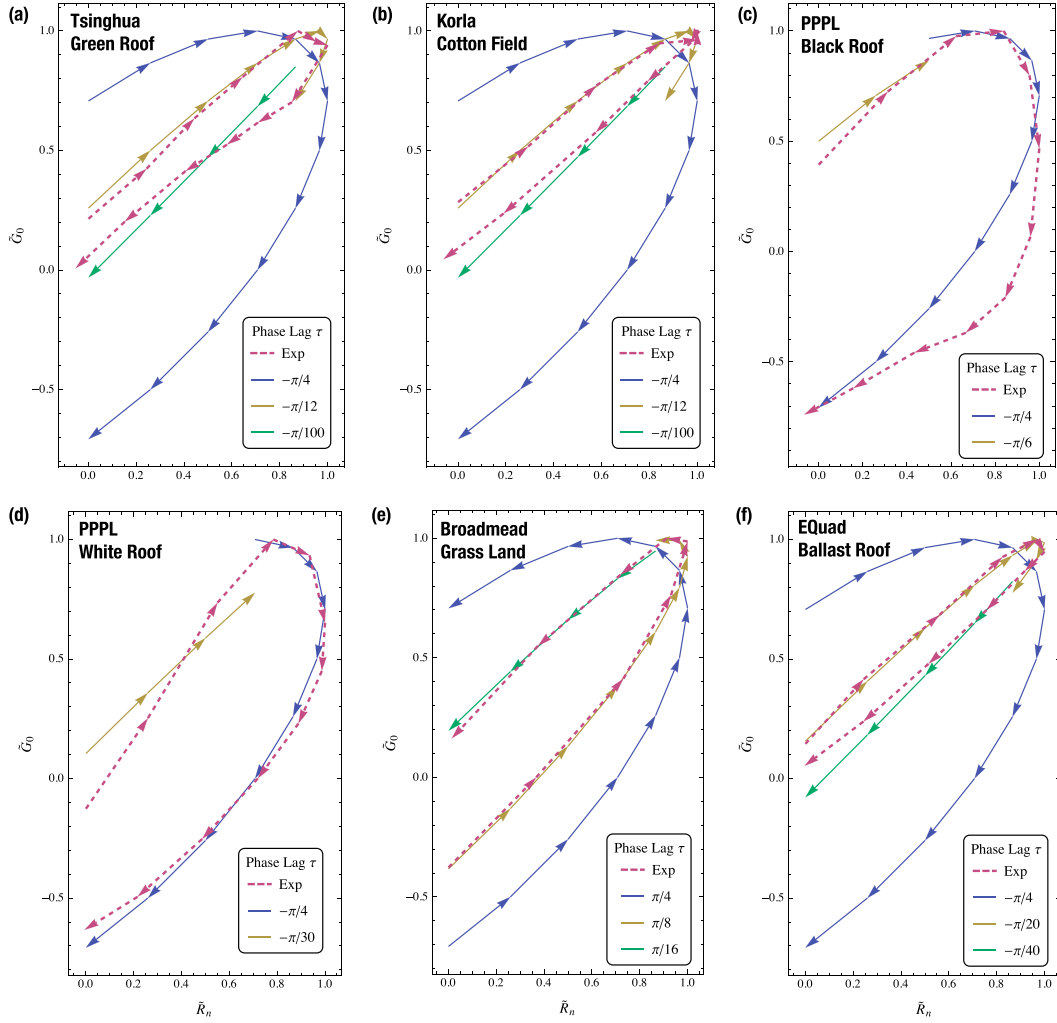
Figure 3. Daytime hysteresis loops between $\widetilde{R}_n$ and $\widetilde{G}_0$ from field measurements at: (a) Tsinghua Green Roof site, (b) Korla Cotton Field site, (c) PPPL Black Roof site, (d) PPPL White Roof site, (e) Broadmead Grass Land site, and (f) EQuad Ballast Roof. Measurement datasets are plotted in dashed lines and the theoretical ones in solid lines. The arrows indicate loop directionality. The information of field measurement sites and sampling dates is provided in Table 1.

$$T(z,t) = A_T \exp(-z/M) \sin(\omega t - \varepsilon - z/N) + \overline{T}s, \qquad (13)$$

$$
\begin{aligned}
G(z,t) &\equiv -\lambda \frac{\partial T}{\partial z} \\
&= \lambda A_T \frac{\sqrt{M^2 + N^2}}{MN} \exp(-z/M) \sin(\omega t - \varepsilon - z/N + \delta),
\end{aligned} \quad (14)
$$

where λ is the soil thermal conductivity, $\Delta = \sqrt{\left(W^2 + \sqrt{W^4 + 16\kappa^2\omega^2}\right)/2}$, $N = \Delta/\omega$, and $M = 2\kappa/(\Delta + W)$. In equation (14),

$$\delta = \arctan\left(\frac{M}{N}\right) = \arctan\left[\frac{2k\omega}{(\Delta + W)\Delta}\right], \qquad (15)$$

is the phase lag of the soil temperature response to the heat flux forcing, which holds at any depth z. In particular, at the surface $z = 0$, the ground heat flux G_0 is given by,

$$G_0(t) = \lambda A_T \frac{\sqrt{M^2 + N^2}}{MN} \sin(\omega t - \varepsilon + \delta), \qquad (16)$$

which can be normalized as

$$\widetilde{G}_0(t) = \sin(\omega t - \varepsilon + \delta). \qquad (17)$$

2.3. Analyzing the Phase Lag Between R_n and G_0

[8] Comparing equations (11) and (17), the phase lag τ between R_n and G_0 is

$$\tau = -(\xi + \delta) + \varepsilon. \qquad (18)$$

$\tau > 0$ implies the phase evolution of $\widetilde{G}_0$ falls behind that of $\widetilde{R}_n$ and vice versa. Of the three contributors to τ, ξ is the phase difference between R_n and S_d; δ is the phase difference between T_s and G_0; and ε is the phase difference between two control parameters T_s and S_d. The three contributors to τ are analyzed term by term as follows:

[9] 1. ξ: By introducing two scaling variables, $A_s^* = (1 - \alpha)A_s$ and $A_T^* = 4\varepsilon_s \sigma T_a^3 A_T$ for the scaled amplitudes of the net shortwave radiation and the outgoing longwave radiation, respectively, equation (9) can be simplified as
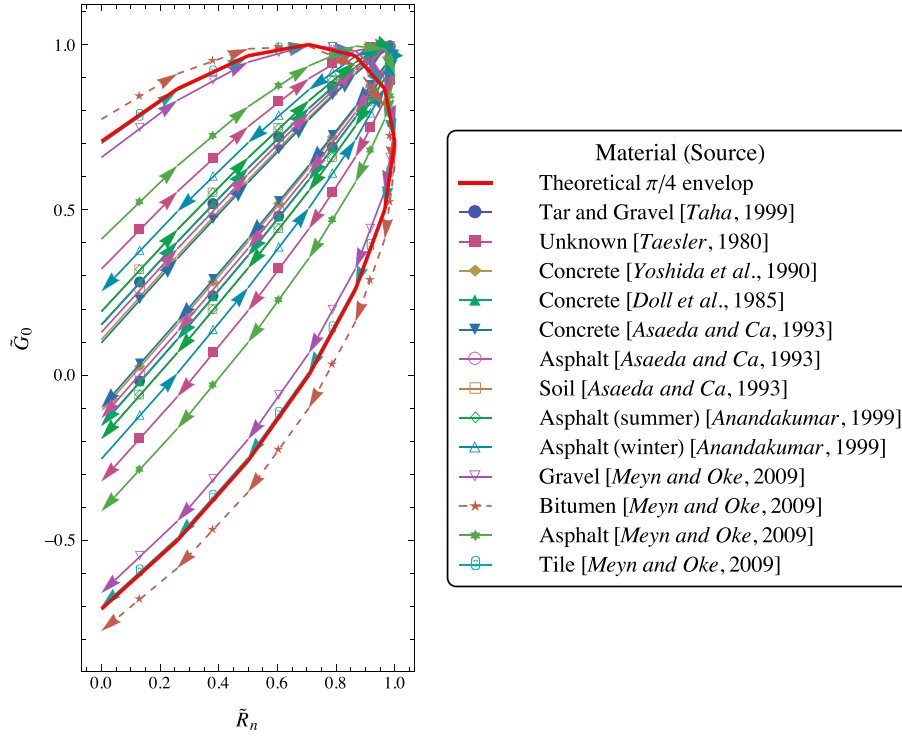
Figure 4. Daytime hysteresis loops between $\widetilde{R}_n$ and $\widetilde{G}_0$ occurred on surfaces of various materials retrieved from the literature. The bold solid red line denotes the theoretical enveloping loop with the limit $\tau = \pm \pi/4$. All hysteresis loops except one reported in the literature fall within the theoretical limit.

$$\xi = \arctan\left(\frac{\sin\varepsilon}{\cos\varepsilon - A_s^*/A_T^*}\right). \quad (19)$$

The ratio A_s^*/A_T^* is a function of T_a with magnitude greater than unity, as shown in Figure 1a. The phase lag ξ varies in the range of

$$-\pi/2 < \xi < 0, \quad (20)$$

according to equation (19) as a function of $A_s^*/A_T^* > 1$, and is plotted in Figure 1b.

[10] 2. δ: From equation (15) [*Gao et al.*, 2003, 2010], δ varies in the range of

$$0 < \delta \leq \pi/4, \quad (21)$$

depending on the soil water flux density W, as shown in Figure 1c. The limiting case $\delta = \pi/4$ is attained for dry soils with water flux $W = 0$. For a given water flux density W, the phase lag δ increases with the thermal diffusivity k as shown in Figure 1d.

[11] 3. ε: As S_d directly drives the SEB system and T_s responds to S_d relatively quickly through surface heating, it is reasonable to assume that the response time of T_s to S_d (represented by ε) is insignificant as compared to the one between S_d and R_n (represented by ξ as indirect response through atmospheric heating), which leads to $\varepsilon \ll \xi$. In addition, the response of T_s to G_0 (represented by δ through soil heating) is also much slower than that of T_s to S_d (represented by ε), leading to $\varepsilon \ll \delta$.

[12] From Figure 1, it is clear that both the scaled ratio A_s^*/A_T^* that indicates ambient forcing intensity, and the water flux density W that is associated with the soil water transport of heat, play crucial roles in dictating the total phase lag τ between $\widetilde{R}_n$ and $\widetilde{G}_0$. In the limiting cases: (a) with strong radiative forcing as $A_s^*/A_T^* \to \infty$, ξ approaches 0; (b) with weak ambient forcing as $A_s^*/A_T^* \to 1$, ξ decreases to $-\pi/2$. Meanwhile, as most available solar energy A_s^* is dissipated by the outgoing longwave radiation A_T^*, the evaporation dominated by the atmospheric demand will be weak, leading to $W \to 0$ and $\delta \to \pi/4$. This is the likely scenario encountered in most field observations especially under clear-sky conditions, which, however, does not exclude the theoretical possibility that evaporation can still occur under the condition $A_s^*/A_T^* \to 1$ in more general settings (e.g., rain on hot pavement surfaces). Applying these limiting cases, and combining equations (18), (20), and (21), we then have a physical range of τ variation, as

$$-\pi/4 < \tau < \pi/4. \quad (22)$$

[13] Given this range, Figure 2 shows that, for a positive τ, the hysteresis loop between diurnal $\widetilde{R}_n$ and $\widetilde{G}_0$ evolves in a counterclockwise direction, and vice versa. Physically, the directionality of hysteresis loops indicates the relative strength of radiative forcing and the soil wetness acting in opposite directions: wider counterclockwise hysteresis loops for stronger radiative forcing and clockwise ones for drier soils. In addition, note that the diurnal variation of soil water flux (or evaporation) is not considered in this study, which

may contribute to the actual phase evolution of surface energy budgets as well.

3. Validation by Field Measurements

[14] To validate our theoretical quantification of the phase lag between $\widetilde{R}_n$ and $\widetilde{G}_0$, we selected field experiment data from six sites with different LULC types (i.e., natural and artificial) and wetness conditions (i.e., wet, moderate, and dry) for comparisons. Note that cloud cover has significant impact on the actual phase evolution of all energy budgets [*Camuffo and Bernardi*, 1982]. Shallow cumulus clouds generate more high frequencies and perturb the main daily harmonic [*Gentine et al.*, 2012]. In this study, we only include data periods with clear days to exclude impacts of cloud cover and precipitation. Due to different instrumentation at each site, we use either energy residual or heat storage method to obtain the ground heat flux G_0. The energy residual is a straightforward way by taking G_0 as the residual of other SEB terms, while the heat storage method estimates G_0 by adding the heat storage above a heat flux plate measurement [*Anandakumar*, 1999]. The magnitude of G_0 computed as the energy residual is inaccurate due to the SEB closure problem [*Foken*, 2008], whereas we assume that the phase evolution is less susceptible. The description of the data sources is given in Table 1.

[15] Notice that actual evolutions of T_s and S_d mimic sinusoidal variation with principle diurnal frequency only during daytime [*Gao et al.*, 2003]. Thus, for field datasets, we rescale R_n and G_0 in the following way: after obtaining the hourly series of R_n and G_0, we first set the daily peak value as the upper limit, and the value observed 5 h prior to the peak as the lower limit. The diurnal series are then normalized by the upper and lower limits, resulting in a rescaled series ranging in [0, 1] (with 0 and 1 corresponding to the lower and upper limits, respectively).

[16] Figure 3 shows normalized daytime hysteresis loops between R_n and G_0 from field measurements, with comparisons to theoretical predictions. All field measurements, except the one in Figure 3e, exhibit clockwise hysteresis loop, indicating G_0 is leading in phase. An explanation of the fact that G_0 is usually leading in phase as compared to R_n is given by *Gentine et al.* [2011]. The hysteresis effect between R_n and G_0, conventionally described using three empirical coefficients, is completely characterized by a single theoretically-derived parameter, viz. the phase difference τ. In particular, for artificial (dry) materials, the theoretical $-\pi/4$ phase difference is successfully recovered in the afternoon loop as shown in Figures 3c and 3d. It is noteworthy that in Figure 3, the morning segments differ from the afternoon ones, which is likely due to the impact of soil water flux uptake. For engineered roofs in Figures 3c and 3d, the morning-afternoon difference can be attributed to evaporation of dew formed on roof surfaces in the morning.

[17] It is also noteworthy that distinguished hysteresis patterns in two adjacent sites (i.e., Broadmead Grass Land and EQuad Ballast Roof sites) are observed in Figures 3e and 3f, respectively. Given the same meteorological conditions at these two sites, the difference in loop patterns, in terms of both directionality and magnitude, reveals the importance of soil water advection in regulating G_0. At Broadmead site (grass land), there is a much stronger water flux density W, as compared to that at EQuad Roof

site (suburban area with $W \rightarrow 0$). As a result, the positive phase lag δ (nearly $\pi/4$ for dry surfaces) at EQuad site effectively offsets the slightly negative phase lag ξ, leading to $\tau = -\xi - \delta < 0$, while at Broadmead site $\tau \approx - > 0$ remains positive as $\delta \rightarrow 0$ due to strong soil water flux advection.

4. Linkage to Camuffo-Bernadi Formula

[18] Here we revisit the Camuffo-Bernadi formula in equation (2) originated from empirical analysis. By substituting equation (7) into equation (2), we have

$$G_0(t) = A_R[a_1 \sin(\omega t - \xi) + a_2 \omega \cos(\omega t - \xi)] + a_3 + a_1 R'_n$$

(23)

Following the previous procedure of normalization, we obtain

$$\widetilde{G}_0(t) = \sin\left(\omega t - \xi - \tau'\right),$$ (24)

where

$$\tau' = \arctan(-a_2\omega/a_1).$$ (25)

It is apparent that τ' in equation (24) is equivalent to the formulation of τ in equation (18), implying $-\pi/4 < \tau' < \pi/4$. With empirical coefficients a_1 and a_2 reported by numerous researchers in the literature, hysteresis loops between normalized R_n and G_0 for land surfaces of various materials are plotted in Figure 4. It is clear that the derived range of τ' from Camuffo-Bernadi formula in equation (24) falls within the theoretical range of $[-\pi/4, \pi/4]$, for all loops except one.

[19] In practice, for any given site, the physical basis of these empirical coefficients a_1 and a_2 can now be characterized to elucidate the phase lag between the two energy budget terms by relating equations (24) and (18), in the light of the present analysis under clear-sky conditions. The remaining coefficient a_3 is characterized as the intercept of a G_0 versus R_n plot (ignored in our analysis through normalization), which is independent of the relative phase evolution of R_n and G_0. The physical interpretation of a_3 therefore requires further investigation.

5. Concluding Remarks

[20] This study provides insight into the governing mechanisms of the hysteresis effect between the ground heat flux and net radiation, based on theoretical characterization of the diurnal phase difference between G_0 and R_n. Our model captures the bi-directional (i.e., clockwise and counterclockwise) patterns of experimentally observed hysteresis loops well. The evaporation-driven soil water flux density W and the radiative forcing ratio A_s^*/A_T^* (net shortwave radiation to outgoing longwave radiation) essentially dictate the shape and directionality of hysteresis loops. The theoretical analysis is validated against field measurements over a wide variety of LULC types. The empirical coefficients in the classic Camuffo-Bernadi model admit physical interpretations in the light of current analysis. Following a similar methodology, the analysis in this study can be potentially extended to develop novel parameterization schemes for computing sensible and latent heat fluxes in the SEB system.

References

Anandakumar, K. (1999), A study on the partition of net radiation into heat fluxes on a dry asphalt surface, *Atmos. Environ.*, *33*(24–25), 3911–3918, doi:10.1016/S1352-2310(99)00133-8.

Asaeda, T., and V. T. Ca (1993), The subsurface transport of heat and moisture and its effect on the environment: A numerical model, *Bound.-Lay. Meteorol.*, *65*(1–2), 159–179, doi:10.1007/BF00708822.

Asaeda, T., V. T. Ca, and A. Wake (1996), Heat storage of pavement and its effect on the lower atmosphere, *Atmos. Environ.*, *30*(3), 413–427, doi:10.1016/1352-2310(94)00140-5.

Bateni, S. M., and D. Entekhabi (2012), Relative efficiency of land surface energy balance components, *Water Resour. Res.*, *48*(4), W04510, doi:10.1029/2011WR011357.

Bhumralkar, C. M. (1975), Numerical experiment on computation of ground surface temperature in an atmospheric general circulation model, *J. Appl. Meteorol.*, *14*(7), 1246–1258.

Brutsaert, W. (1975), On a derivable formula for long-wave radiation from clear skies, *Water Resour. Res.*, *11*(5), 742–744, doi:10.1029/WR011i005p00742.

Camuffo, D., and A. Bernardi (1982), An observational study of heat fluxes and their relationships with net radiation, *Bound.-Lay. Meteorol.*, *23*(3), 359–368, doi:10.1007/BF00121121.

Chen, F., and J. Dudhia (2001), Coupling an advanced land surface-hydrology model with the Penn State-NCAR MM5 modeling system. Part I: Model implementation and sensitivity, *Mon. Weather Rev.*, *129*(4), 569–585, doi:10.1175/1520-0493(2001)129<0569:CAALSH>2.0.CO;2.

Doll, D., J. Ching, and J. Kaneshiro (1985), Parameterization of subsurface heating for soil and concrete using net radiation data, *Bound.-Lay. Meteorol.*, *32*(4), 351–372, doi:10.1007/BF00122000.

Foken, T. (2008), The energy balance closure problem: An overview, *Ecol. Appl.*, *18*(6), 1351–1367. doi:10.1890/06-0922.1.

Gao, Z., R. Horton, and H. P. Liu (2010), Impact of wave phase difference between soil surface heat flux and soil surface temperature on soil surface energy balance closure, *J. Geophys. Res.*, *115*(D16), D16112, doi:10.1029/2009JD013278.

Gao, Z., X. G. Fan, and L. G. Bian (2003), An analytical solution to one-dimensional thermal conduction-convection in soil, *Soil Sci.*, *168*(2), 99–107, doi:10.1097/01.ss.0000055305.23789.be.

Gentine, P., D. Entekhabi, and B. Heusinkveld (2012), Systematic errors in ground heat flux estimation and their correction, *Water Resour. Res.*, *48*(9), W09541, doi:10.1029/2010WR010203.

Gentine, P., D. Entekhabi, and J. Polcher (2010), Spectral behaviour of a coupled land-surface and boundary-layer system, *Bound.-Lay. Meteorol.*, *134*(1), 157–180, doi:10.1007/s10546-009-9433-z.

Gentine, P., J. Polcher, and D. Entekhabi (2011), Harmonic propagation of variability in surface energy balance within a coupled soil-vegetation-atmosphere system, *Water Resour. Res.*, *47*(5), W05525, doi:10.1029/2010WR009268.

Grimmond, S., H. A. Cleugh, and T. R. Oke (1991), An objective urban heat storage model and its comparison with other schemes, *Atmos. Environ. B-Urban*, *25*(3), 311–326, doi:10.1016/0957-1272(91)90003-W.

Humes, K. S., W. P. Kustas, and M. S. Moran (1994), Use of remote sensing and reference site measurements to estimate instantaneous surface energy balance components over a semiarid rangeland watershed, *Water Resour. Res.*, *30*(5), 1363–1373, doi:10.1029/93WR03082.

Katul, G. G., R. Oren, S. Manzoni, C. Higgins, and M. B. Parlange (2012), Evapotranspiration: a process driving mass transport and energy exchange in the soil-plant-atmosphere-climate system, *Rev. Geophys.*, *50*(3), RG3002, doi:10.1029/2011RG000366.

Kustas, W. P., and C. S. T. Daughtry (1990), Estimation of the soil heat flux/net radiation ratio from spectral data, *Agric. For. Meteorol.*, *49*(3), 205–223, doi:10.1016/0168-1923(90)90033-3.

Liang, X., D. P. Lettenmaier, E. F. Wood, and S. J. Burges (1994), A simple hydrologically based model of land surface water and energy fluxes for general circulation models, *J. Geophys. Res.*, *99*(D7), 14415–14428, doi:10.1029/94JD00483.

Mccumber, M. C., and R. A. Pielke (1981), Simulation of the effects of surface fluxes of heat and moisture in a mesoscale numerical model. 1. Soil Layer, *J Geophys. Res. Ocean Atmos.*, *86*(Nc10), 9929–9938, doi:10.1029/JC086iC10p09929.

Meyn, S. K., and T. R. Oke (2009), Heat fluxes through roofs and their relevance to estimates of urban heat storage, *Energy Build.*, *41*(7), 745–752, doi:10.1016/j.enbuild.2009.02.005.

Ren, T., G. J. Kluitenberg, and R. Horton (2000), Determining soil water flux and pore water velocity by a heat pulse technique, *Soil Sci. Soc. Am. J.*, *64*(2), 552–560.

Santanello, J. A., and M. A. Friedl (2003), Diurnal covariation in soil heat flux and net radiation, *J. Appl. Meteorol.*, *42*(6), 851–862, doi:10.1175/1520-0450(2003)042<0851:DCISHF>2.0.CO;2.

Sellers, P. J., et al. (1997), Modeling the exchanges of energy, water, and carbon between continents and the atmosphere, *Science*, *275*(5299), 502–509, doi:10.1126/science.275.5299.502.

Sun, T., E. Bou-Zeid, Z.-H. Wang, E. Zerba, and G.-H. Ni (2013), Hydrometeorological determinants of green roof performance via a vertically-resolved model for heat and water transport, *Build. Environ.*, *60*(C), 211–224, doi:10.1016/j.buildenv.2012.10.018.

Taesler, R. (1980), *Studies of the development and thermal structure of the urban boundary layer in Uppsala. Part 1: Experimental program and Part 2: Data analysis and results. Rep. 61*, Uppsala Universitetet, Uppsala, Sweden, 236 pp.

Taha, H. (1997), Urban climates and heat islands: albedo, evapotranspiration, and anthropogenic heat, *Energy Build.*, *25*(2), 99–103, doi:10.1016/S0378-7788(96)00999-1.

Wang, Z.-H., and E. Bou-Zeid (2012), A novel approach for the estimation of soil ground heat flux, *Agric. For. Meteorol.*, *154–155*, 214–221, doi:10.1016/j.agrformet.2011.12.001.

Wang, Z.-H., E. Bou-Zeid, and J. A. Smith (2011), A Spatially-Analytical Scheme for Surface Temperatures and Conductive Heat Fluxes in Urban Canopy Models, *Bound.-Lay. Meteorol.*, *138*(2), 171–193, doi:10.1007/s10546-010-9552-6.

Yoshida, A., K. Tominaga, and S. Watatani (1990), Field measurements on energy balance of an urban canyon in the summer season, *Energy Build.*, *15*(3–4), 417–423, doi:10.1016/0378-7788(90)90016-C.